SEMARAK ILMU PUBLISHING

CFD Letters

Journal homepage:
https://semarakilmu.com.my/journals/index.php/CFD_Letters/index
ISSN: 2180-1363

Cooling Strategies for Heated Cylinders Using Pulsating Airflow with Different Waveforms

Mohamed A. Aziz[1,*], Mostafa E. El-Salamony[2], Ernesto Benini[3], Osama A. Gaheen[4], Mohamed. A. Khalefa[4]

[1] College of Engineering, Suez University, Suez, Egypt
[2] College of Engineering, Peking University Beijing, No.5 Yiheyuan Road, Haidian District, Beijing 100871, P.R.China
[3] University of Padoua, Via 8 Febbraio 1848 2 - 35122 Padova, Italy
[4] Institute of Aviation Engineering and Technology, 35CQ+2GC, Al Matar, Imbaba, Giza Governorate 3811302, Giza, Egypt

ARTICLE INFO

Article history:
Received 26 October 2022
Received in revised form 24 November 2022
Accepted 21 December 2022
Available online 1 September 2023

Keywords:
Pulsating Flow; Pulsating Wind Tunnel; Heated Cylinder; Optimization; Cooling; Regression Analysis

ABSTRACT

Pulsate flow is an effective technique applied for cooling several engineering systems depending on their pulsate frequency. One very sound external flow pulsation application is heat transfer over heated bodies. In present work, an experimental design and numerical model of controlled pulsating flow according to generated pulsating frequency and wave shape around a heated cylinder were performed. The effects of pulsating frequency, amplitude, and mean velocity on the fluid flow and heat transfer characteristics over a heated cylinder were studied. The wave frequency varied from 2 to 12 Hz, and the amplitude varied from 0.2 to 0.8 m/s. Moreover, different waveforms were investigated to determine their effect on wall cooling. For constant wave frequency and amplitude, the most efficient wave in cooling was the sawtooth wave, with the average wall temperature after 30 s was 1.6 °C cooler than that of the forced convection case, followed by the triangular wave at 1.2 °C less. The heat transfer rate and the flow field were drastically influenced by the variations of these parameters. Optimization was conducted for each wave type to find the optimum wave frequency and amplitude. The optimizing showed that, the most efficient wave was the sawtooth with 12°C temperature reduction compared with that of the forced convection case, followed by the triangular. Furthermore, regression analysis was conducted to estimate the relationships between these variables and surface temperature. It was found that the wave amplitude had a greater role in cooling than that of the frequency.

1. Introduction

External unsteady convection heat transfer mode on heated bodies such as cylinders is very effective technique in real engineering life, for example, parallel and counter flow in heat exchanger applications. Now a day, the latest research in literatures has shown sensitivity of heat transfer improvement to pulse flow mode. The problem of a cylinder in pulsating crossflow was introduced in many applications through the literature. One such application introduced the lagged behavior of

* *Corresponding author.*
E-mail address: mohamed.aziz@suezuni.edu.eg (Mohamed A. Aziz)

https://doi.org/10.37934/cfdl.15.9.5682

the heat release of a heated wire in crossflow in a tube that turns heat into sound, known as the Rijke tube [1]. Another application is hot wire anemometry, the dynamic behavior of which is of great interest [2].

Recently researchers have paid attention to the heat transfer characteristics from a cylinder subjected to pulsating flow using numerical simulation and experiments. Yu *et al.,* [3] conducted a computational fluid dynamics CFD study for flow pulsation over cylinder with square cross section. The study included heat transferee investigations for different pulsation amplitude and frequency. Their conclusions showed increment of heat transfer at lock on frequency (vortex shedding natural frequency). Molochnikov *et al.,* [4] offered flow pulsation analysis around cylinder. They proposed correction factor that may be applied for heat transfer correlation of simple flow across cylinders. Saxena and Ng [5] produced a CFD investigations of flow pulsation across heated cylinder. Their results evaluated the flow shedding frequency while interacting with cylinders of several aspect ratios. Bhalla and Dhiman [6] presented numerical models for flow pulsation mode compared to continuous flow mode over heated half-cylinder inside a channel. Their findings showed an increment in Nusselt number by 10% due to use of flow pulsation. Li *et al.,* [7] experimentally investigated that heat transfer coefficient across heated cylinder improved by using pulsate flow. On the other hand, the experimental work showed that the heat transfer reduces with low pulsating frequencies while it increased with increasing the pulsating frequency. Ji *et al.,* [8] studied experimental flow pulsation of air flow around heated cylinder. Their conclusions revealed improvement of heat transfer especially at 'lock-on' frequency of pulsation. Kikuchi *et al.,* [9] performed experimental investigation for flow pulsation around a heated cylinder. Their results showed that the flow separation near the beck cylinder half improved the heat transfer at that zone. Perwaiz and Base [10] introduced an experimental study for flow pulsation around a heated cylinder with surface temperature. Their conclusions revealed a sensitive relation between heat transfer and pulsation frequency. Where the heat transfer decreases for low frequency and increase for high frequency of pulsation.

Flow pulsation has been widely utilized in heat transfer improvement. In electronic engineering field with the development of electronic equipment to deal with very high thermal loads it is crucial to get effective and consistent cooling techniques [11,12]. Fluid pulsation has been proven to improve heat transfer due to phenomena such as turbulence, intermittent mixing, and dynamic change of thermal boundary layer [13-16]. Thus, in latest years, investigations of pulsating flows to improve heat transfer efficiency have got encouraging interest [14,17-19]. Recent research recommends that pulsating flow is favorable for the application of pulsating crossflow through a cylinder or other objects [20-24]. Farahani *et al.,* [25] Inspected the effect of the pulsating flow jet on the thermal and vibrational performance of the cylinder. Compared with the efficiency of the steady jet. The most important parameters examined include pulsing jet velocity and frequency. Esfe *et al.,* [26] present summary of pulsating flow without and with heat transfer and the effects of nanofluids are considered. Using pulsating flows instead of steady flows are effective approach in improving heat transfer. Ye *et al.,* [27] presents experimental results concerning heat transfer performance of cross pulsating flow around a cylinder and concentrates on heat transfer characteristics improvement gotten using a new and unusual kind of pulse method capable of produce varying pulsate waves with various frequencies. Mladin and Zumbrunnen [28] Have performed experimental study of flow pulsations effect on the heat transfer characteristics of a two-dimensional air jet where the Nusselt numbers in the mid-plane increased to 80%. Poh *et al.,* [29] have performed numerical study of flow pulsations effect on Nusselt number under a laminar impinging jet. the greatest heat transfer enhancement with the combination of Re = 300, f = 5 Hz and H/d = 9. Coulthard *et al.,* [30] have studied experimentally the pulsate film cooling effectiveness on heat transfer using solenoid valves

to generate flow pulsation where pulsing with high frequency improved film-cooling effectiveness by lowering the jet liftoff.

The next section presents the research on pulsed flow, considering the waveform of the pulses and their effect on the heat transfer characteristics. Xu *et al.,* [31] have introduced experimental investigation of pulsating flow ambitious by variety of wave signals and study the Effects of pulsating flow parameters on heat transfer characteristics. They have studied square, triangular, sawtooth, and sinusoidal wave signal. Their results showed that the square wave leads to a more average flow rate and improved heat transfer characteristics under the same pulsating frequency compared to the other three waves.

In a previous study, Li *et al.,* [32] investigated rectangular wave (R-wave) and triangular wave (T-wave) impingement with nanofluid periodic pulsating slot-jet. They analyzed the effects of the jet waveform, pulsation frequency from 10 to 50 Hz, and Reynolds number from 10,000 to 20,000 on heat transfer enhancement. The frequency induced a trend effect on the heat transfer enhancement.

Zargarabadi *et al.,* [33] performed a numerical simulation for pulsating impinging jet on an asymmetrical concave surface where a sinusoidal pulsation was formed based on the average velocity for regular impingement supplied to the concave surface. They investigated the effects of frequency, pulsation amplitude, relative curvature, nozzle-to-surface distance, jet displacement, and Reynolds number on the flow and heat transfer characteristics. Their results indicated that changing the pulsation frequency within the range of 40 to 160 Hz increased the time-averaged Nusselt number by 2%–8%. Meanwhile, Zhang *et al.,* [34] numerically studied the various waveforms (sinusoidal, rectangular, and triangular) applied to a confined two-dimensional slot jet impinging on a heated plate for heat transfer improvement and compared the results with those for a steady air jet. The Reynolds numbers varied from 1553 to 7766, the frequency varied from 10 to 400 Hz, the Strouhal number varied from 0.012 to 2.4, and the jet-to-surface distances ranged from 2 to 8. The best heat transfer performance was achieved using triangular jets at its critical Strouhal number St = 0.24–0.48. A higher heat transfer rate than those of other cases at the same Re was achieved.

Geng *et al.,* [35] applied a designed periodic air to a heated surface to enhance heat transfer in comparison with those of steady air jets. The experiments featured triangular, sinusoidal, and rectangular jets with frequencies that ranged from 1.25 to 20 Hz. The results showed some beneficial influence on heat transfer improvement and that the improvement of the combined signals lay between the performances of the individual signals. The sinusoidal or triangular plus shapes demonstrated some enhanced performance compared with the rectangular plus shape. Mohammadpour *et al.,* [36] numerically investigated the effects of sinusoidal and square-wave-shaped flow pulsations on the heat transfer rate from a slot jet impinging on a concave surface. In their study, the frequency varied from 20 to 80 Hz, the pulse amplitude from 0.2 to 1.0, and the Reynolds number from 4740 to 7200. The studied square wave shape showed higher rates of heat transfer compared with those of the sinusoidal wave shape. The pulsated jet flow caused a higher heat transfer rate than that of the steady jet flow. The enhancement of the local Nusselt number was associated with the increase in jet Reynolds number. Increasing the pulsation frequency improved the average rate of heat transfer.

Mladin and Zumbrunnen [37] experimentally investigated the effect of flow pulsations on the local heat transfer characteristics of a planar air jet. Their results showed that using pulse amplitudes within the range of 0% to 50% of the mean flow velocity and pulsation frequencies corresponded to Strouhal numbers lower than 0.106, which increased the Nusselt numbers in the nozzle mid-plane by 12%–80%. Mladin and Zumbrunnen [38] implemented a boundary layer model to ascertain the effects of the pulse shape, frequency, and amplitude on the heat transfer in a planar stagnation region. Their results indicated that the interaction of the frequency and amplitude and the

nonlinearity of the governing equation reduced the time averaged Nusselt number by up to 16%. Sheriff and Zumbrunnen [39] experimentally investigated the influence of flow pulsations on local heat transfer on an impinging water jet. They considered sinusoidal and square-pulse wave shapes. The pulse amplitude varied from 0.5% to 100% of the mean-to-peak velocity, whereas the pulse frequencies varied from 5 to 280 Hz.

Demircan and Turkoglu [40] numerically analyzed the characteristics of a sinusoidally oscillating jet impinging on a flat surface. They studied the effects of jet oscillation amplitude, frequency, and Reynolds number on the flow and heat transfer characteristics. They concluded that the Nusselt number relatively increased when the jet oscillated compared with that of a steady jet. Bazdidi-Tehrani *et al.,* [41] analyzed oscillatory flow impinging on a disc and its effect on heat transfer characteristics. Their results showed an enhancement of heat transfer and a reduction of Nusselt number fluctuation with increasing oscillation frequency from 16 to 400 Hz. Recent research has paid attention to boundary conditions setup for investigation of environmental wind profile, simulation of synthetic jet cooling, fluid and structure analysis using ANSYS, meshing for CFD modelling, cooling of hot cylinder in backward-facing step channel and effect of the isothermal fins on the natural convection heat transfer where the contributions of such researches have very important rule in in understanding and defining correct setup for the boundary conditions and turbulent models suitable for the problem [42-47].

It is clear from the foregoing and what has been referred to in the literature that there is no accurate and clear study on the effect of the wave form on the heat transfer coefficient by studying the effect of wave form control parameters such as amplitude and frequency. The current research presents this study accurately to reach the optimal wave shape used in cooling of cylinder in cross air flow and their proposed properties such as frequency and amplitude. This paper aimed to study heat transfer over a heated cylinder using different inlet air velocity waveforms, determine the effects of the waveform, amplitude, mean value, and frequency, and find the most efficient cooling way in terms of the waveform, amplitude, and frequency. These are explored as follows. The problem setup is discussed in Section 2 and validated in Section 3, where the experimental setup is mentioned. Results of the heat transfer and aerodynamic characteristics for different waveforms are discussed in Section 4, followed by the determination of the optimum frequency and amplitude and analysis of these data through regression modeling in Section 5. Finally, the article is concluded in Section 6.

2. Problem Setup

2.1 Experimental Apparatus and Procedure

The experimental work was carried out through our apparatus [48,49]. The tunnel was equipped with a flow pulsation generator, Figure 1. Table 1 includes the tunnel specifications.

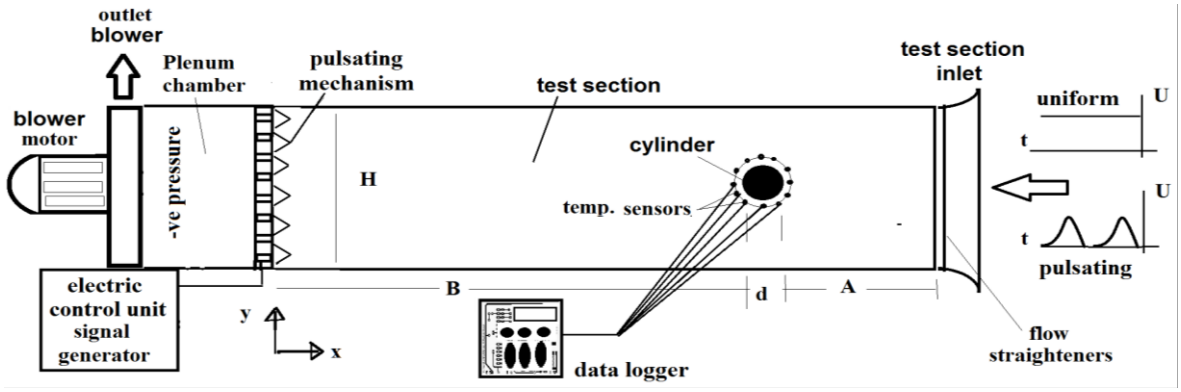

Fig. 1. Pulsating flow apparatus

Table 1
Tunnel specifications

Test section	Dimensions
Cross section	Square 200mm×200mm
length	1600 mm
Reynolds number	1~2 ×10^4
Pulse frequency	1~12 Hz

2.2 Numerical Modeling

A computational model setting was conducted according to the problem definition [48,50]. The CFD computations were performed, and convergence was determined based on the decrease in temperature of wall after three minutes. There are fifteen inflation layers around the cylinder with a growth rate of 1.15, and the cylinder was divided into 100 elements. The body of the influence growth rate was 1.1. The different meshes are listed in Table 2. It can be seen that, except for the coarsest mesh, the average wall temperature tended to a certain value as the mesh got finer, as shown in Figure 2. Moreover, the internal grid sensitivity was checked through the temperature distribution over the cylinder, as shown in Figure 3.

Table 2
Different tested meshes

	Mesh 1	Mesh 2	Mesh 3	Mesh 4	Mesh 5
Number of nodes	29336	33984	44478	72237	247350
Number of elements	69841	83720	115401	197847	809764
Average quality	0.44018	0.45491	0.50883	0.64235	0.7804
Standard deviation	0.25109	0.22753	0.20151	0.18038	0.14679
Temperature (K)	379.29	379.335	378.955	378.91	378.614

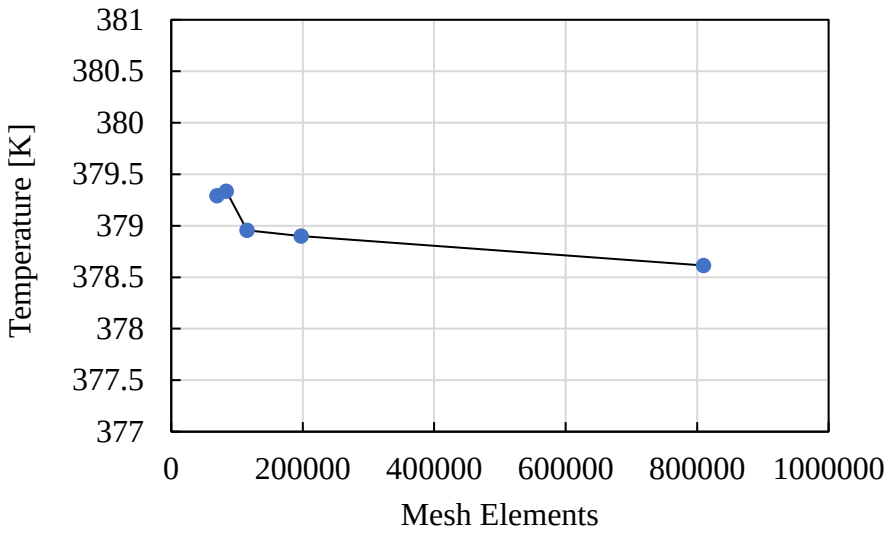

Fig. 2. Number of elements vs. average wall temperature for different meshes

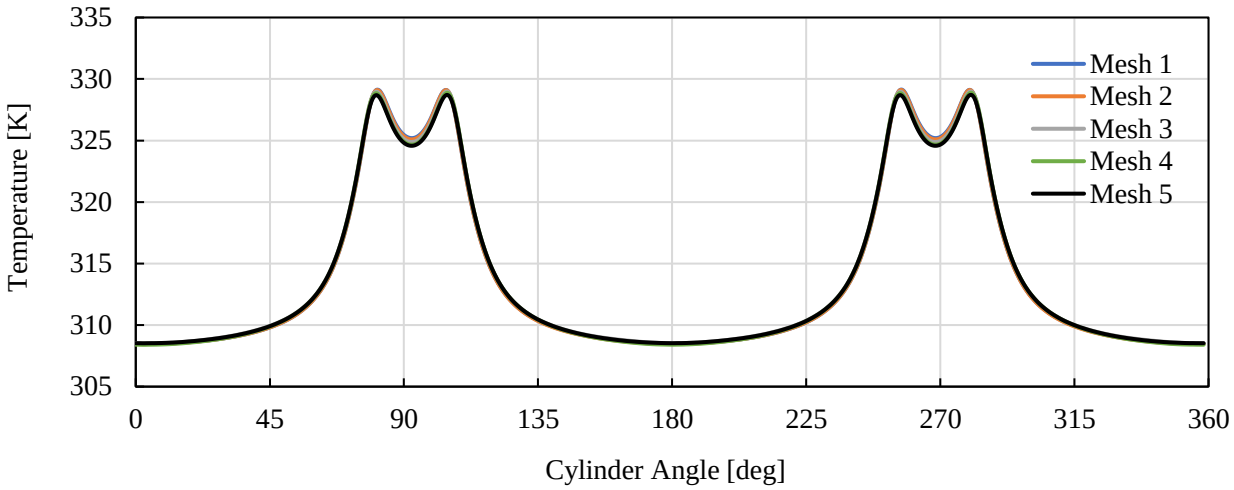

Fig. 3. Cylinder wall temperature distribution for different meshes

After the examination of the meshes, Mesh 3 was chosen. The mesh around the cylinder is shown in Figure 4, and its properties are summarized in Table 3. A temperature difference of 1.3K was found by comparing the temperature reduction herein with that in the experimental results, where the temperature reduction after 5 min was 9.3K. This difference can be tuned based on the wind tunnel wall temperature.

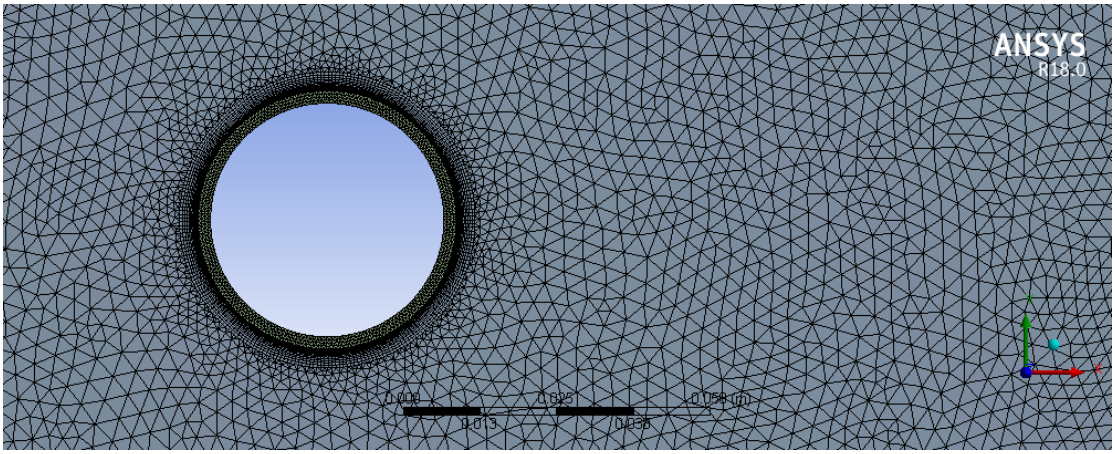

Fig. 4. Mesh grid around cylinder surface

Table 3
Properties of the used mesh

Property	Value
Nodes	44478
Elements	115401
Average quality	0.50883
Standard deviation	0.20151
Wall sizing	250
Inflation layers	15
Inflation growth rate	1.15
Body of influence sizing	3.00E−03 m
Body of influence growth rate	1.1

2.3 Numerical Boundary Conditions

Considering the physics of the problem, the cylinder initial temperature is maintained at 105°C. The inlet velocity follows Eq. (1).

$$V = V_{\text{mean}} + V_{\text{amp}} \times |\sin(\omega t)| \tag{1}$$

where both V_{mean} and V_{amp} are 1 m/s, and ω varies from 1 to 12 Hz. The boundary conditions are summarized in Table 4.

Table 4
Boundary conditions

Boundary	Type	Value
Upper and lower walls	No-slip wall	T = 105°C
Side walls	Symmetric	
Inlet	Velocity-inlet	V: Eq. (1)
		T = 25°C
Exit	Pressure exit	Gauge pressure = 0 Pa
		T = 25°C
Cylinder	No-slip wall	Material: Steel
		Qin = 33 W
		Initial T = 105°C

2.4 Validation of the Computational Model

The temperature reduction was compared with those in the experiments, for cases of 1 and 6 Hz, after 5 and 10 min to validate the computational model. The numerical simulation had good accuracy, where the difference ranged from 2°C to 3°C, as shown in Table 5. This error may have been due to the wind tunnel wall temperature as it had a role in the cooling rate of the cylinder. Figure 5 shows the computed and measured average Nusselt number of different pulse frequencies. The results show good qualitative agreement for a wide range of pulse frequencies. The quantitative difference was due to the mismatch in the cooling time between the computational fluid dynamics (CFD) and the experiment—the CFD results were obtained after 3 min, whereas the experimental ones were obtained after 10 min.

Table 5
Comparison between experimental measurement and computational results

Frequency (Hz)	Temperature drop (°C) per 5 minutes			Temperature drop (°C) per 10 minutes		
	numerical simulation	Jena and Gairola [42] and Ariffin and Ahmad [43]	Deviation	numerical simulation	Jena and Gairola [42] and Ariffin and Ahmad [43]	Deviation
low	10.7	9.3	1.4	15.9	12.9	2.1
High	12.4	14.5	3	18.3	21.5	3.2

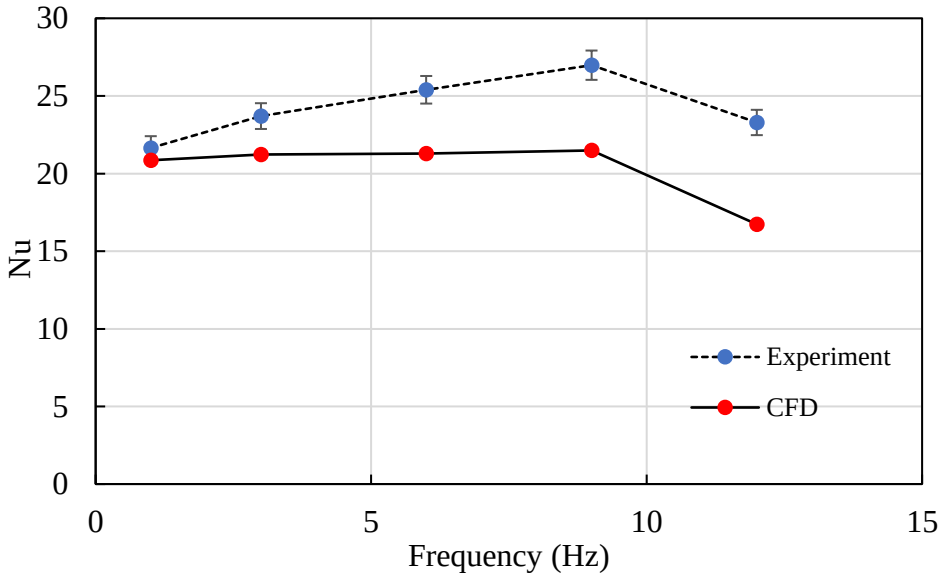

Fig. 5. Computed and measured average Nusselt number of different pulse frequencies

3. Investigated Waves

The inlet velocity was represented as a time-dependent variable to find the best strategy for the inlet air for cooling. Different waves were investigated (i.e., sawtooth, triangular, sine, and square waves) and compared with the forced convection case (i.e., the time-independent velocity). The independent variables of each wave were the mean velocity, wave amplitude, and frequency. These waves are represented in Eq. (2) to Eq. (6) and Figure 6. The square and sine waves were investigated with zero-mean velocity to investigate the zero-net mass flow cooling, so the mass injected in the

first half cycle was taken back in the other half cycle. Hence, a zero-net mass flow was realized. These cases are indexed hereafter as “square/sine zero-mean” waves.

Steady (forced convection): $V = V_{\text{mean}}$ (2)

Sine wave: $V = V_{\text{mean}} + V_{\text{amp}} \times \sin(\omega t)$ (3)

Square wave: $V = V_{\text{mean}} + V_{\text{amp}} \times \text{sign}(\sin(\omega t))$ (4)

Triangular wave: $V = V_{\text{mean}} + V_{\text{amp}} \times \sin^{-1}(\sin(\omega t))$ (5)

Sawtooth wave: $V = V_{\text{mean}} + V_{\text{amp}} \times \tan^{-1}(\tan(\omega t))$ (6)

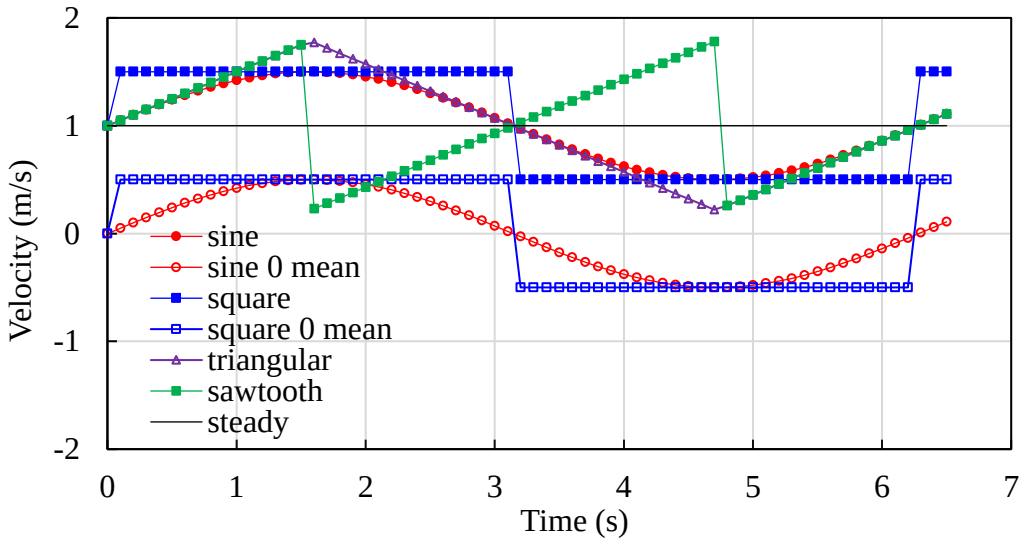

Fig. 6. Velocities of different wave types

4. Results

Because the inlet velocity varied with time, the wake behind the cylinder was unconventional, and the shedding changed its behavior dramatically. The velocities were analyzed using Fourier transform to determine the most energetic frequency and its corresponding energy content to investigate the frequencies in the domain inlet and the wakes behind the cylinder. Seven waveforms with the same frequency and amplitude (0.8 m/s) were investigated. The measurements were recorded at 10 cm from the domain inlet and 11 cm after the cylinder, which corresponded to upstream and downstream positions.

4.1 Heat Transfer Characteristics for Different Waves

The time history of the average wall temperature, shown in Figure 7, indicates how the variable waves affected the heat transfer over the cylinder. The cooling rate of the sawtooth wave in the first few seconds is slow and then increases till it surpasses the other cases. Also, it shows almost no oscillations with time. Meanwhile, the sine, triangular, and square waves show oscillations with time, whereas the zero-mean waves do not. One notable thing is that the heat dissipation rate of the sine wave is better than that of the square wave; however, when the mean velocity decreases to zero,

the square wave shows a better heat dissipation rate. Yet, all the zero-mean waves have heat dissipation rates less than that of the forced convection (steady) case. As mentioned earlier, heat flux is continuously added to the inner cylinder wall along the simulation time. The average wall temperatures of the cylinder after 30 s and the differences in wall temperature with respect to the steady case are listed in Table 6.

Table 6
Average wall temperatures for different waveforms after 30 s

Wave type	Temperature (K)	Temperature difference with respect to the steady case (K)
Steady	378.28	0.00
Triangle	377.09	−1.19
Square	377.49	−0.79
Square zero mean	379.30	1.02
Sawtooth	376.68	−1.60
Sine	377.09	−1.19
Sine zero mean	380.12	1.84

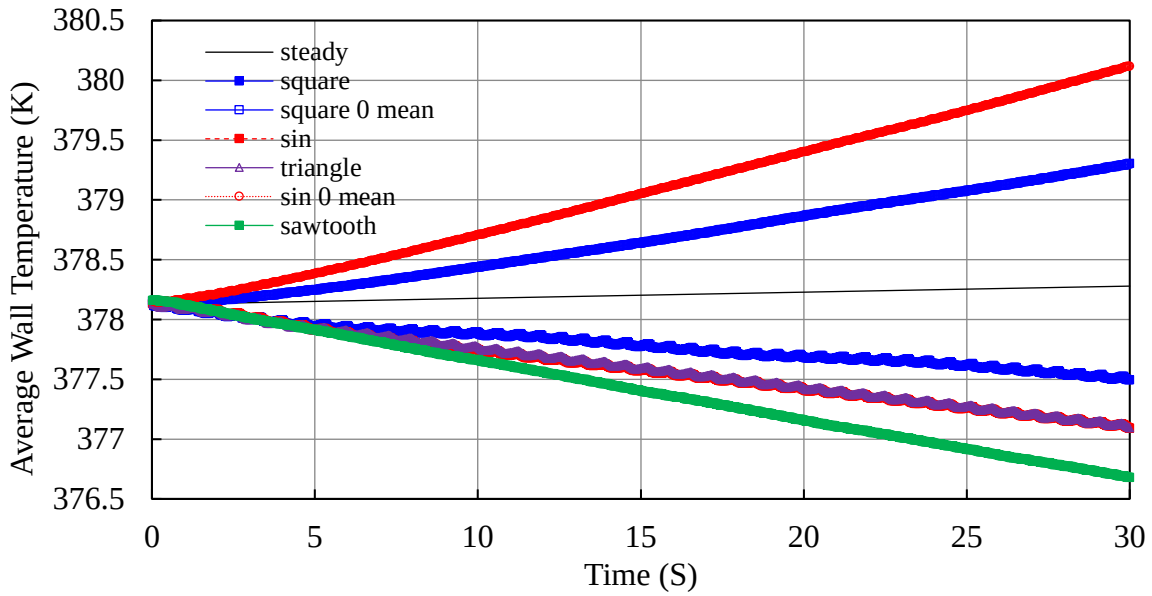

Fig. 7. Time history of the average wall temperature

4.2 Temperature Distribution over the Cylinder Surface

Considering the temperature distribution over the cylinder surface, the forced convection shows two high-temperature zones centered at 90°, each one containing two peaks (see Figure 8). Figure 9 plots the temperature distribution versus the wall angle for different time steps of one wave period ζ. This temperature variation is about 20K. As for the sawtooth and sin waves, shown in Figure 9 and Figure 10, there were two high-temperature peaks at 145° and 330°. The temperature ranges were 0.5K and 1.5K for the sawtooth and sine waves, respectively. For all the above mentioned cases, the temperature range may have changed slightly with time, but the qualitative temperature distribution was time independent.

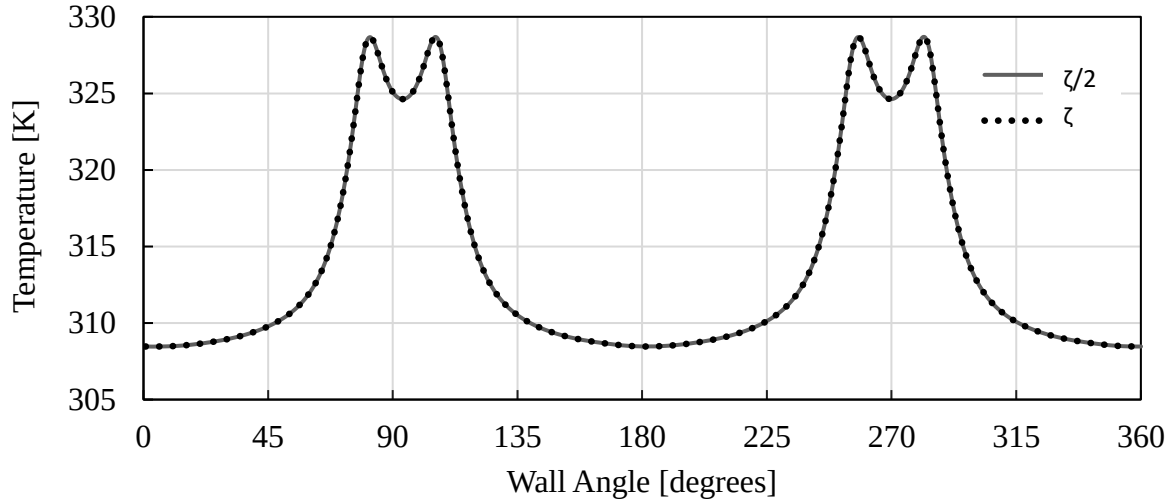

Fig. 8. Temperature distribution over the cylinder surface for forced convection at different time steps

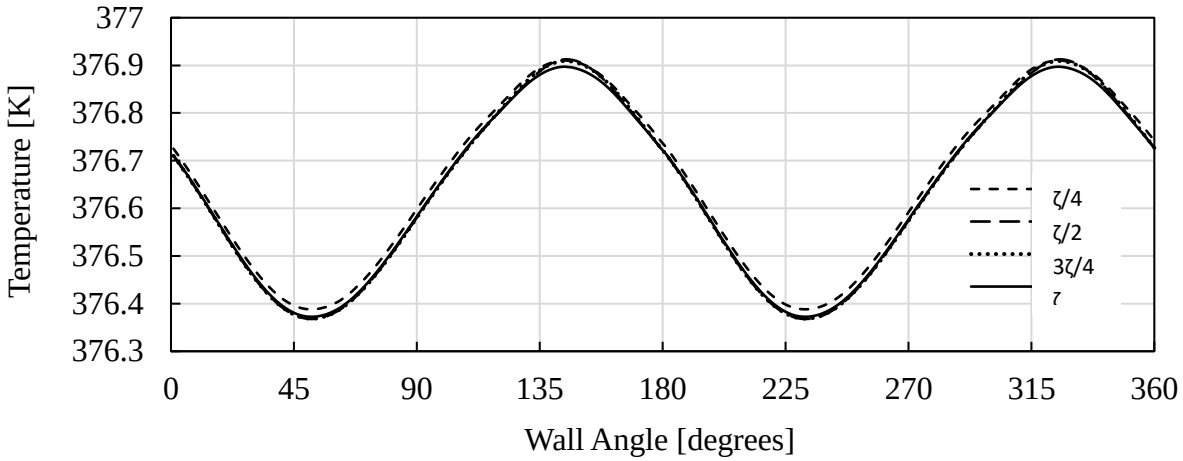

Fig. 9. Temperature distribution over the cylinder surface for the sawtooth waveform at different time steps

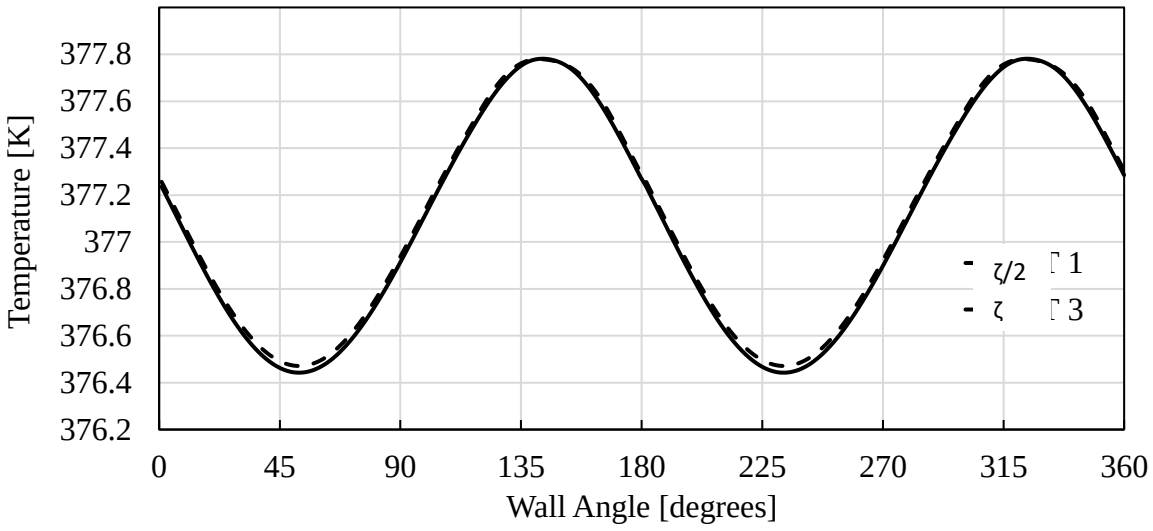

Fig. 10. Temperature distribution over the cylinder surface for the sine waveform at different time steps

For the square and triangular waves, the temperature distribution changed drastically with time. The distribution initially shows two high-temperature zones. Then, the peaks increased in amplitude and then developed into two-headed peaks, as in the steady case. Later, these two-headed peaks spread and became cooler and finally collapsed into two one-headed zones. These peaks are centered at 95° and 275°. The temperature range was 25K for both waves, as shown in Figure 11 and Figure 12.

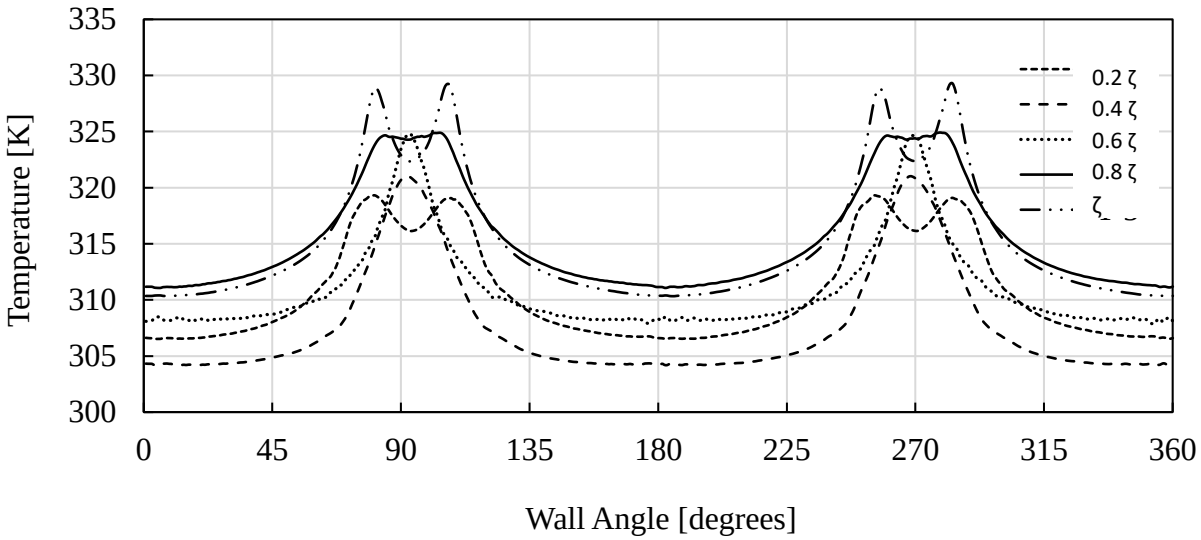

Fig. 11. Temperature distribution over the cylinder surface for the square waveform at different time steps

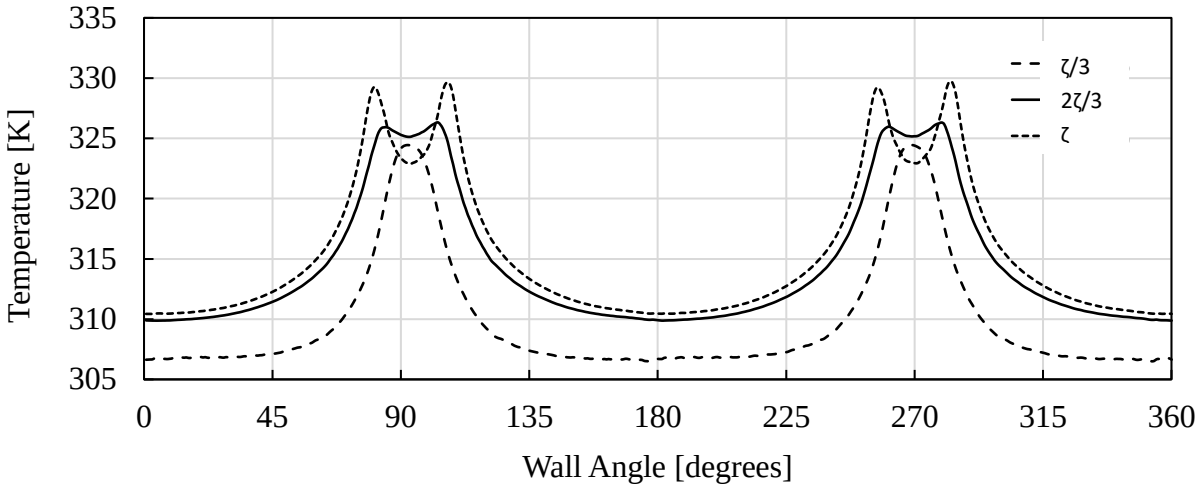

Fig. 12. Temperature distribution over the cylinder surface for the triangular waveform at different time steps

For the square wave with zero-mean velocity, shown in Figure 13, two high-temperature zones changed their loci periodically from 90° and 270° to 0° and 180°. Initially, the peak at 180° decreased its amplitude and spread in both circumferential directions. Then the temperatures gradually increased around the new loci, keeping the centers as low-temperature peaks. Notably, for the distributions centered at 90° and 270°, the average temperature was higher than those of the other distributions. The same qualitative behavior can be observed for the sine wave with zero-mean velocity, shown in Figure 14, except for the peak shape. In this case, the two-headed peak is not

symmetric as one head is more amplified than the other. The temperature ranges were 25k and 20K for the zero-mean square and zero-mean sine waves, respectively.

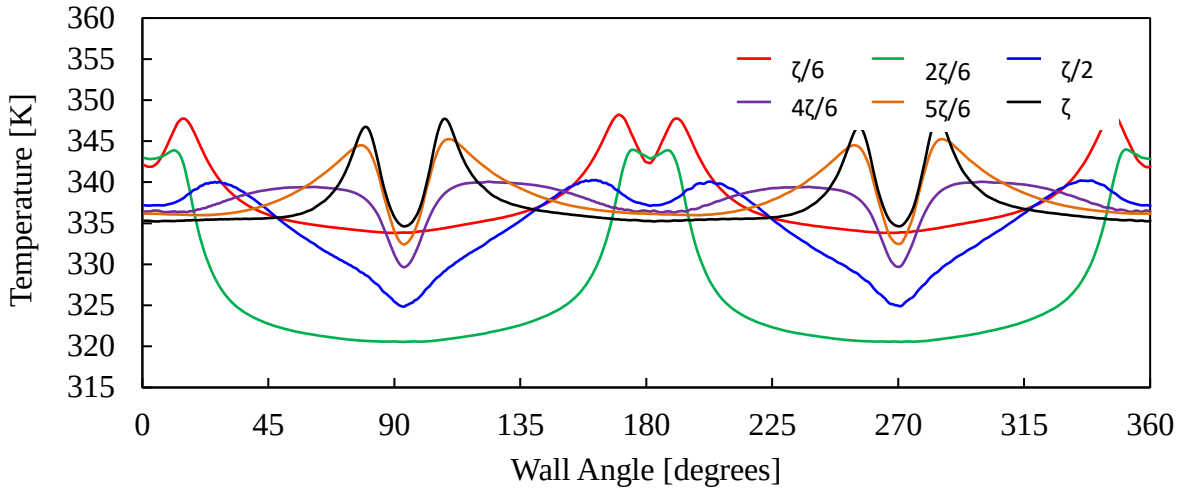

Fig. 13. Temperature distribution over the cylinder surface for the zero-mean square waveform at different time steps

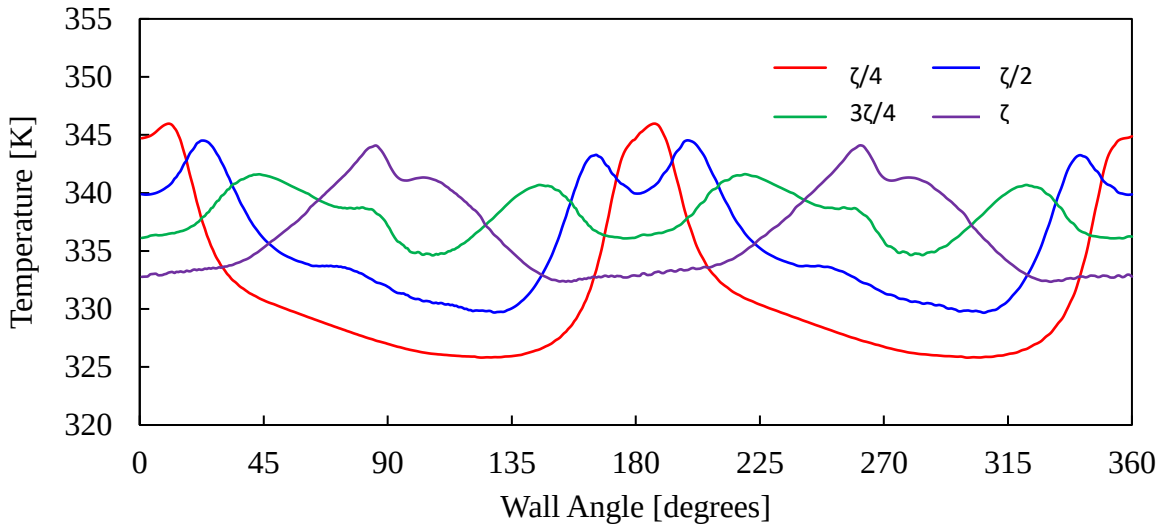

Fig. 14. Temperature distribution over the cylinder surface for the zero-mean sine waveform at different time steps

4.3 Wake Analysis for Different Waves

For the steady flow, there were no frequencies upstream, while there was an extremely weak one downstream at a value of 0.43 Hz. The velocity contour was constant over time, as shown in Figure 15. Hence, vortex shedding was not captured here. Physically speaking, the interference between the wind tunnel walls and the cylinder prevented the formation of the shedding. After enlarging the distance between the wall and the cylinder, the shedding appeared.

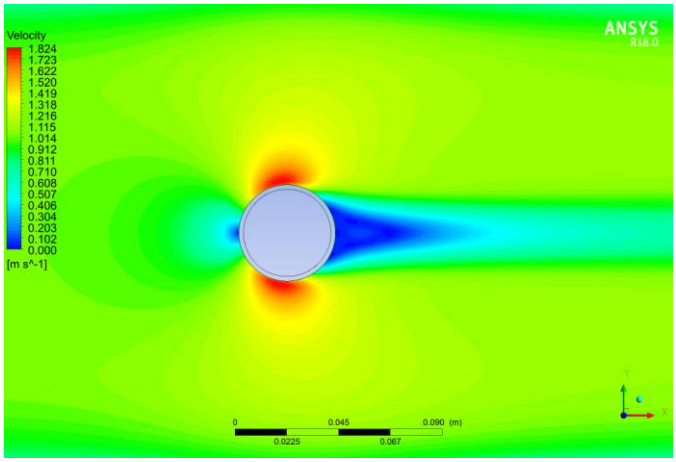

Fig. 15. Velocity field for the steady case

In the case when the inlet velocity changed according to the sawtooth function (Eq. (6)), the maximum amplified frequency was 3.03 Hz, with a power density of 4.83 m^2/s. This corresponds to the first harmonic of the input frequency. Besides, the primary and second harmonic frequencies appeared as well but with very low strength. Downstream, the most amplified frequency was also 3.03 Hz, but its amplitude was seven times less. The harmonics almost vanished both upstream and downstream. By investigating the velocity field, it is observed that when the inlet velocity increased, the cylinder formed an unsymmetrical wake like the vortex shedding behind a cylinder. As the velocity decreased, the same flow pattern was conserved, as shown in Figure 16.

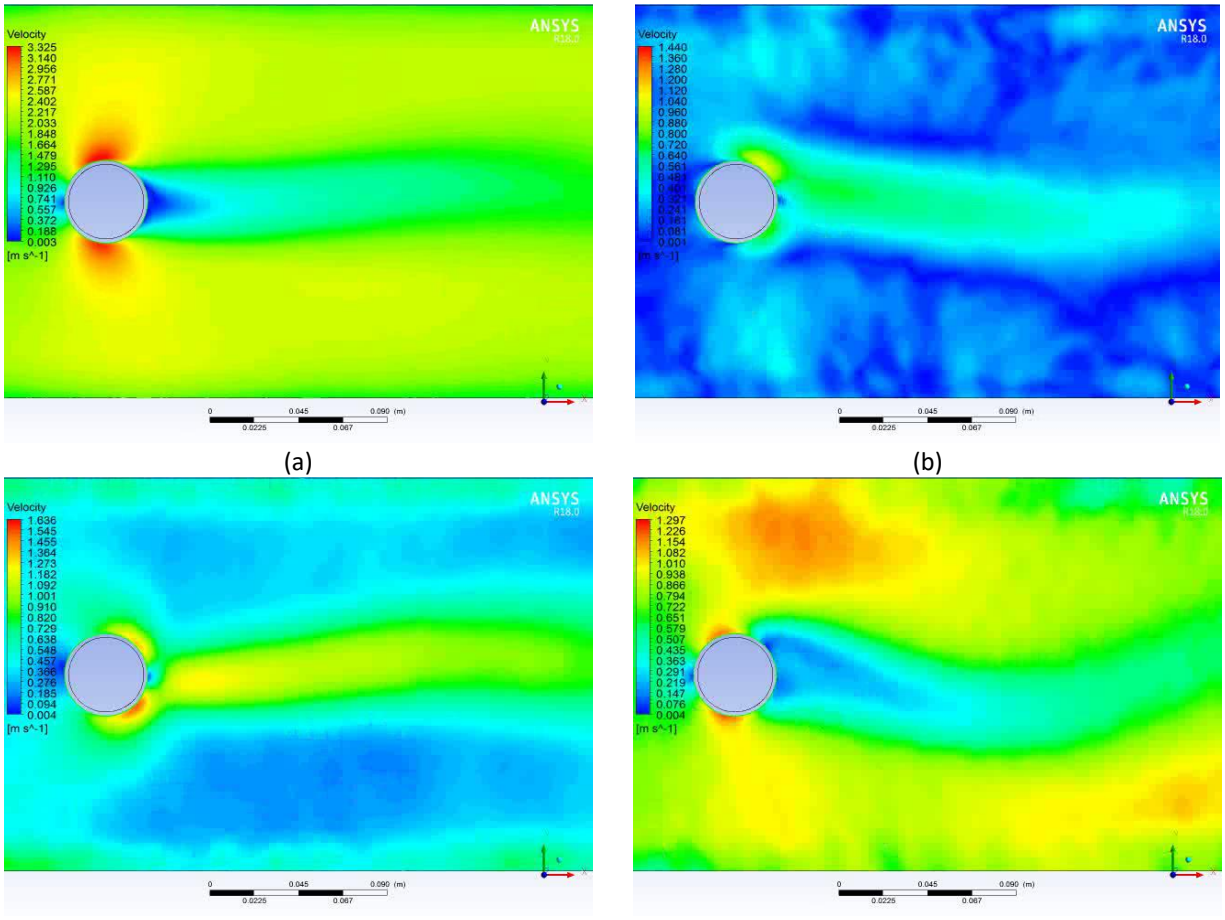

Fig. 16. Velocity field for the sawtooth wave at different time steps; (a) ζ/4, (b) ζ/2, (c) 3ζ/4, (d) ζ

For the triangular-wave inlet flow, the maximum amplified frequency was 1.50 Hz, matching the primary wave frequency. The power density of 8.77 m^2/s was reached, which was twice that of the sawtooth case. Downstream, the same frequency was excited, but its power density was 3.04 m^2/s. This means that the wake here is stronger compared with that of the sawtooth. The first and second harmonics existed upstream, whereas only the first harmonic appeared downstream, with a very small value also. The wakes here were symmetric and did not show shedding. As shown in Figure 17, the wave length was inversely proportional to the inlet velocity. When the inlet velocity decreased, the wake looked like a convergent–divergent wake.

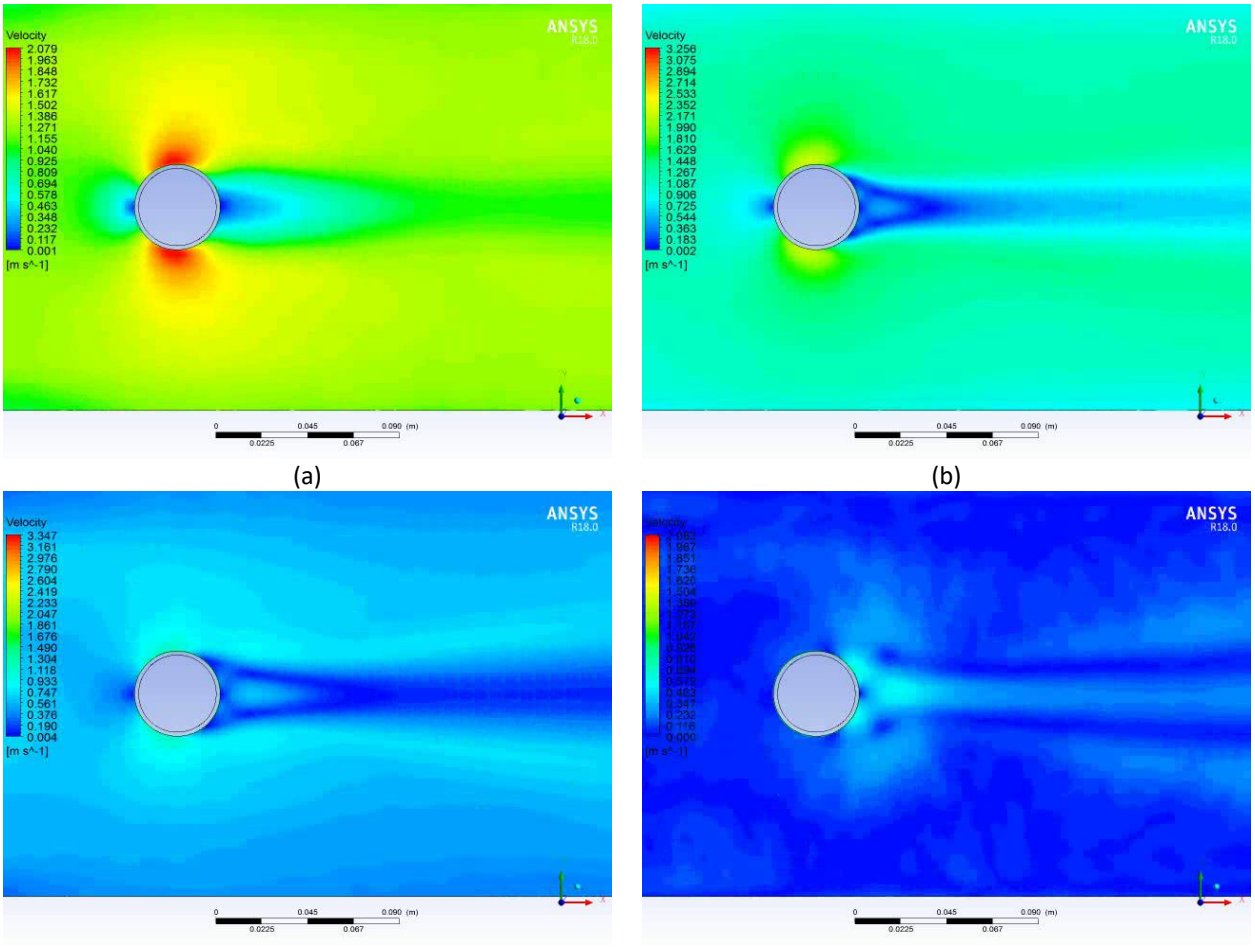

Fig. 17. Velocity field for the triangular wave at different time steps; (a) ζ/4, (b) 2ζ/4, (c) 3ζ/4, (d) ζ

Considering sine wave-inlet velocity, the most amplified frequency in the domain inlet was 1.50 Hz, with a power density of 8.97 m^2/s, which was the highest among all other cases. Downstream, the fundamental frequency was also the most excited one, with a power density of 3.14 m^2/s, which is three times less compared with the upstream one. The harmonics existed in the upstream position with a rather small amplitude but vanished downstream. The wake properties behind the cylinder showed the same characteristics as those for the triangular wave, but the wake was relatively longer, as shown in Figure 18. Also, a larger convergent–divergent wake form appeared when the inlet speed decreased.

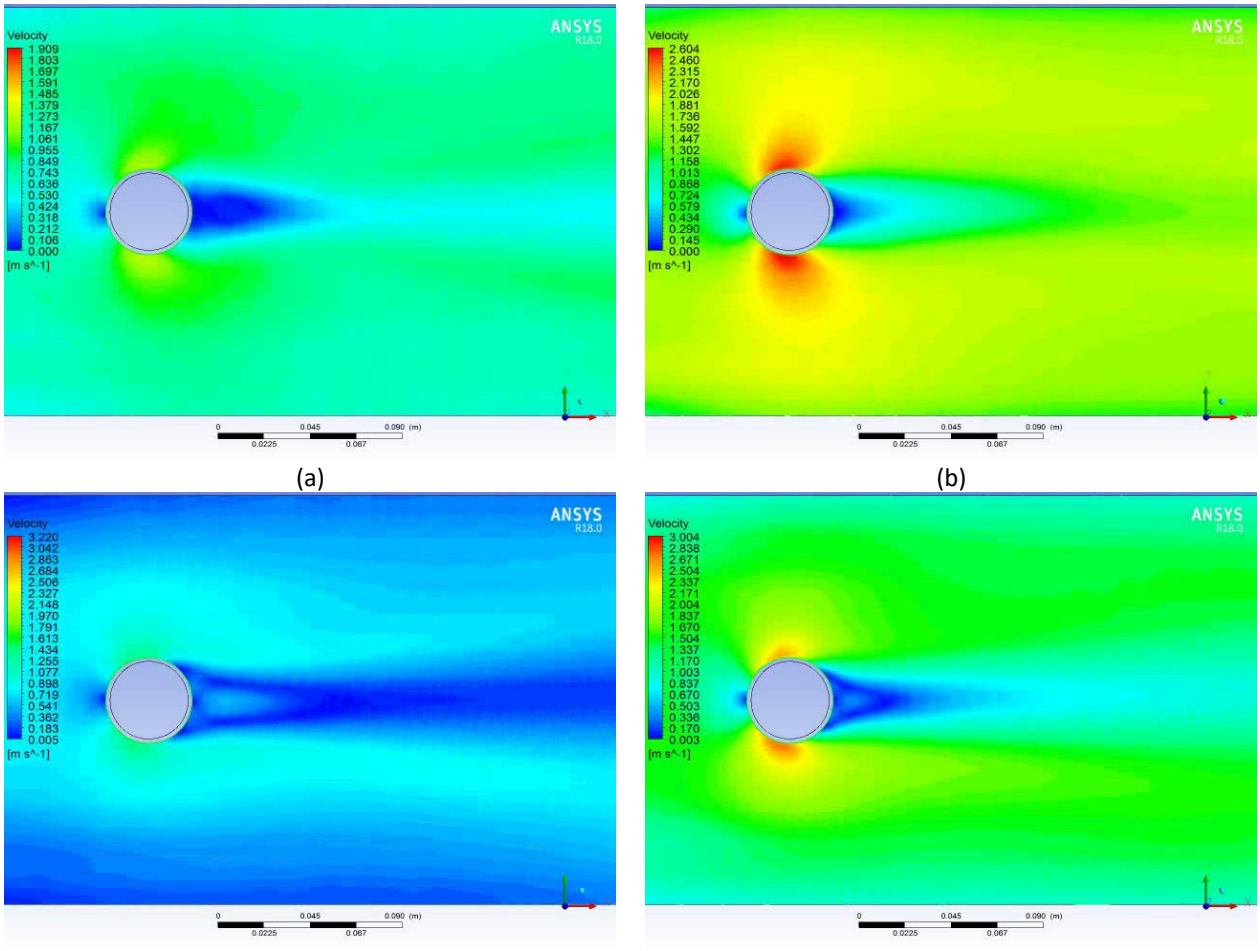

Fig. 18. Velocity field for the sine wave at different time steps; (a) ζ/4, (b) ζ/2, (c) 3ζ/4, (d) ζ

For the same sine wave but setting the mean velocity to zero, the most active frequency jumped to the first harmonic with a power density of 2.57 m^2/s, which was four times less compared with the non-zero-mean sine wave. Meanwhile, downstream of the cylinder, the power spectral density decreased to 1.54 m^2/s, which was only half that of the non-zero-mean sine wave. Besides, although the other harmonics were weaker, they were relative relatively more important with respect to the other sine case. The wakes in this case were also symmetric but shorter. Also, once they appeared behind the cylinder, the airflow reversed its direction; hence, a wake was formed in front of the cylinder with the same characteristics, as shown in Figure 19.

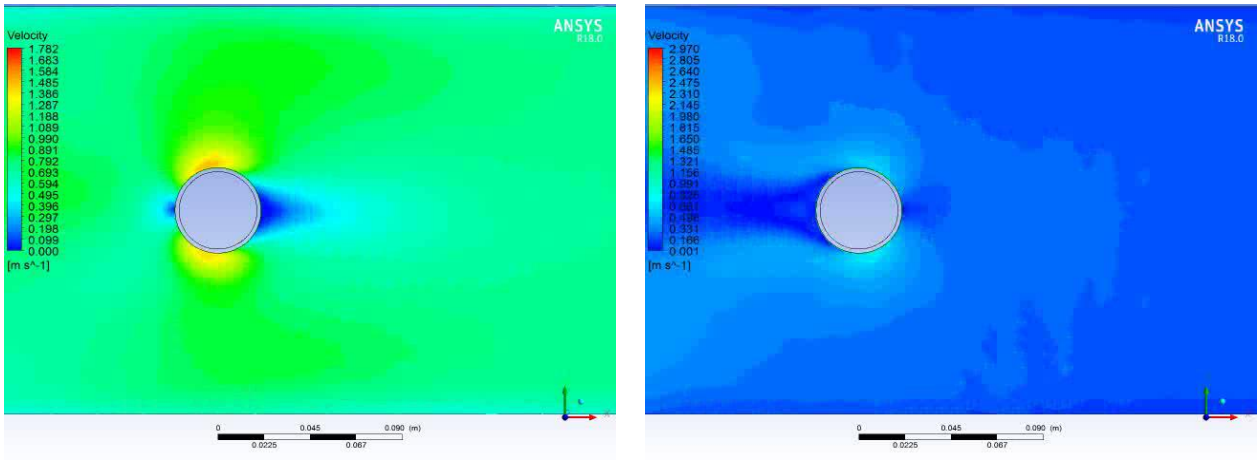

(a) (b)

Fig. 19. Velocity field for the zero-mean sine wave at different time steps; (a) ζ/2, (b) ζ

For the square-wave inlet flow, the maximum amplified frequency was the fundamental one, with a power density of 7.70 m^2/s. Downstream, the same frequency was excited, but its power density was 3.44 m^2/s, which was the highest among all investigated cases. This means that this wave created the most energetic conditions for the wake. The first and second harmonics existed both upstream and downstream. Here the velocity changed suddenly from high to low values. Hence, the wakes started to develop behind the cylinder and grew. The sudden change in the inlet speed made the wake separate and increased the vorticity all over the domain, as shown in Figure 20.

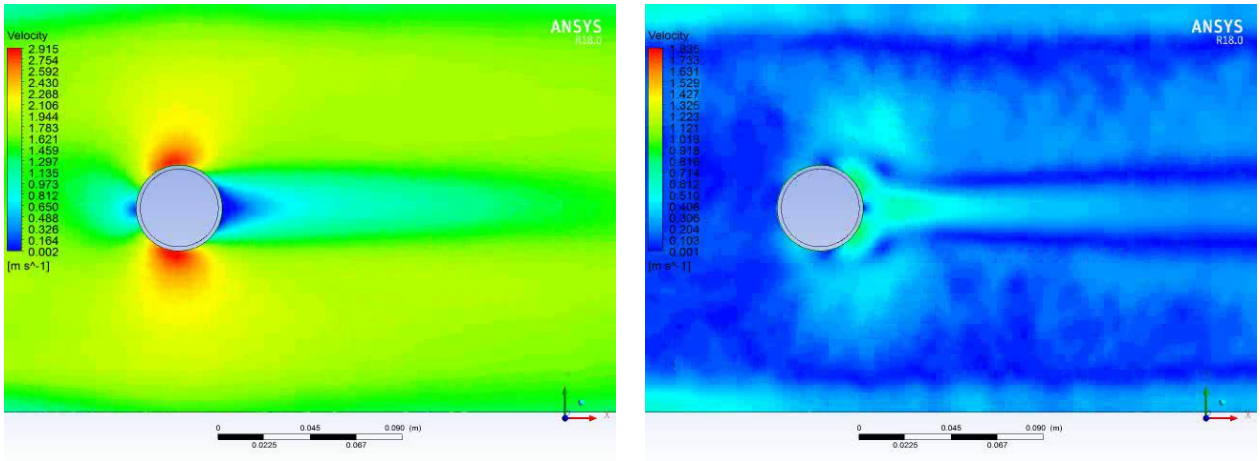

(a) (b)

Fig. 20. Velocity field for the square wave at different time steps; (a) ζ/2, (b) ζ

By decreasing the mean velocity to zero, the most amplified frequency jumped to be the first harmonic one, with a slightly less power density of 7.42 m^2/s. Downstream, the power density reached 0.46 m^2/s, which was relatively too small. Contradicting the zero-mean sine wave, the fundamental frequency in the case of the zero-mean square wave was more energetic than the second harmonic. The wakes here were like those for the sine zero-mean wave but had more time to develop. Consequently, when the flow reversed its direction, the wake breakdown was more chaotic and a slight dissimilarity appears, as shown in Figure 21.

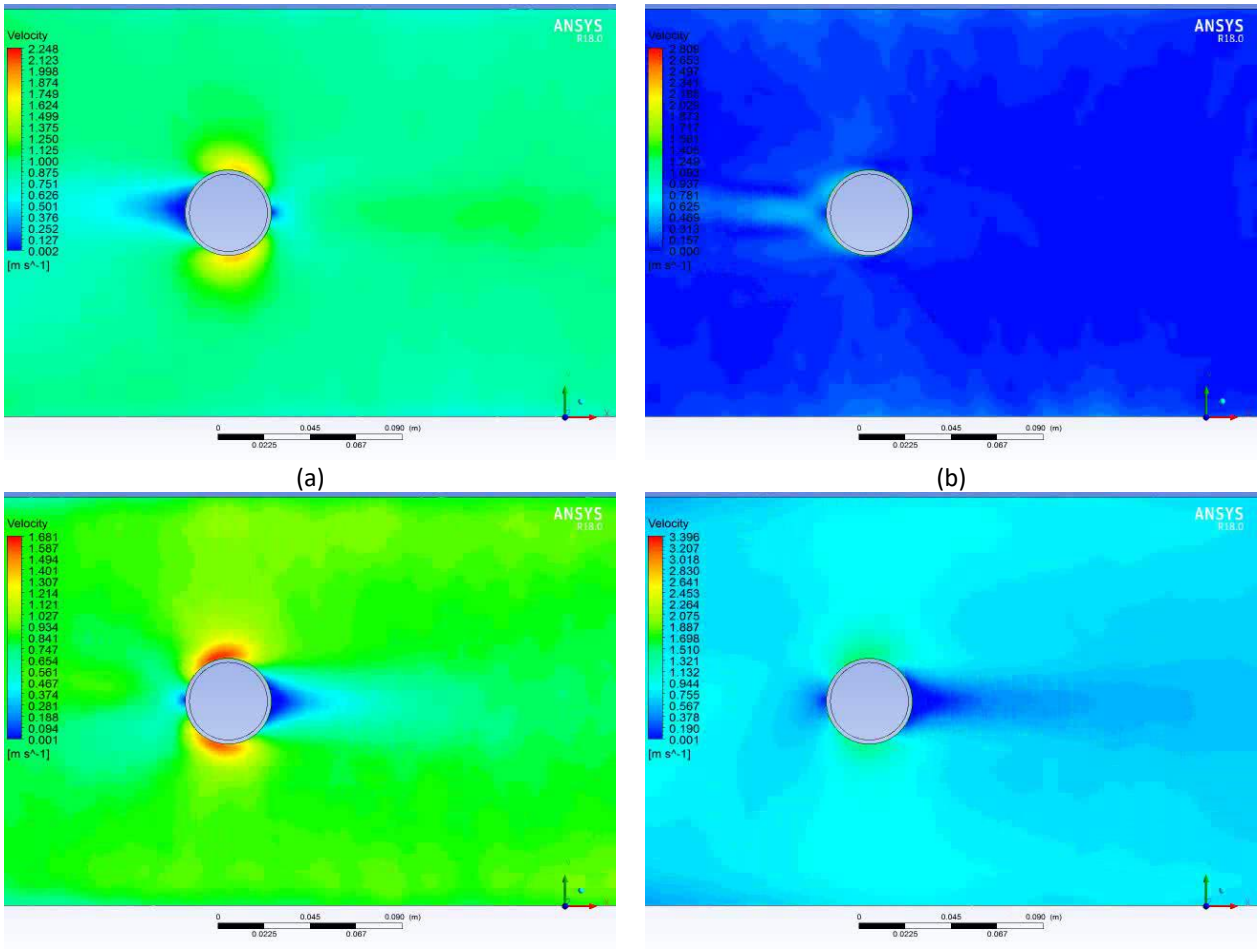

Fig. 21. Velocity field for the zero-mean square wave at different time steps; (a) ζ/4, (b) ζ/2, (c) 3ζ/4, (d) ζ

Hence, one can conclude that the advection speed had a key role in the most energetic frequency in the case where the inlet air was unsteady. That is, it shifted the most energetic frequency from the fundamental to the first harmonic one and reduced the energy content in the cylinder wake. The results are shown in Figure 22 and summarized in Table 7.

Table 7
Frequency analysis of the velocity domain inlet and downstream of the cylinder for the investigated waves

Wave type	Upstream		Downstream	
	Frequency (Hz)	Power spectral density	Frequency (Hz)	Power spectral density
Steady	—	—	0.432878	0.000736
Sawtooth	3.030144	4.834027	3.030144	0.650923
Triangle	1.498423	8.772278	1.498423	3.042085
Sine	1.498423	8.978565	1.498423	3.144493
Sine zero mean	3.030144	2.566781	3.030144	1.54088
Square	1.498423	7.696311	1.498423	3.441833
Square zero mean	3.030144	7.428604	6.060287	0.461602

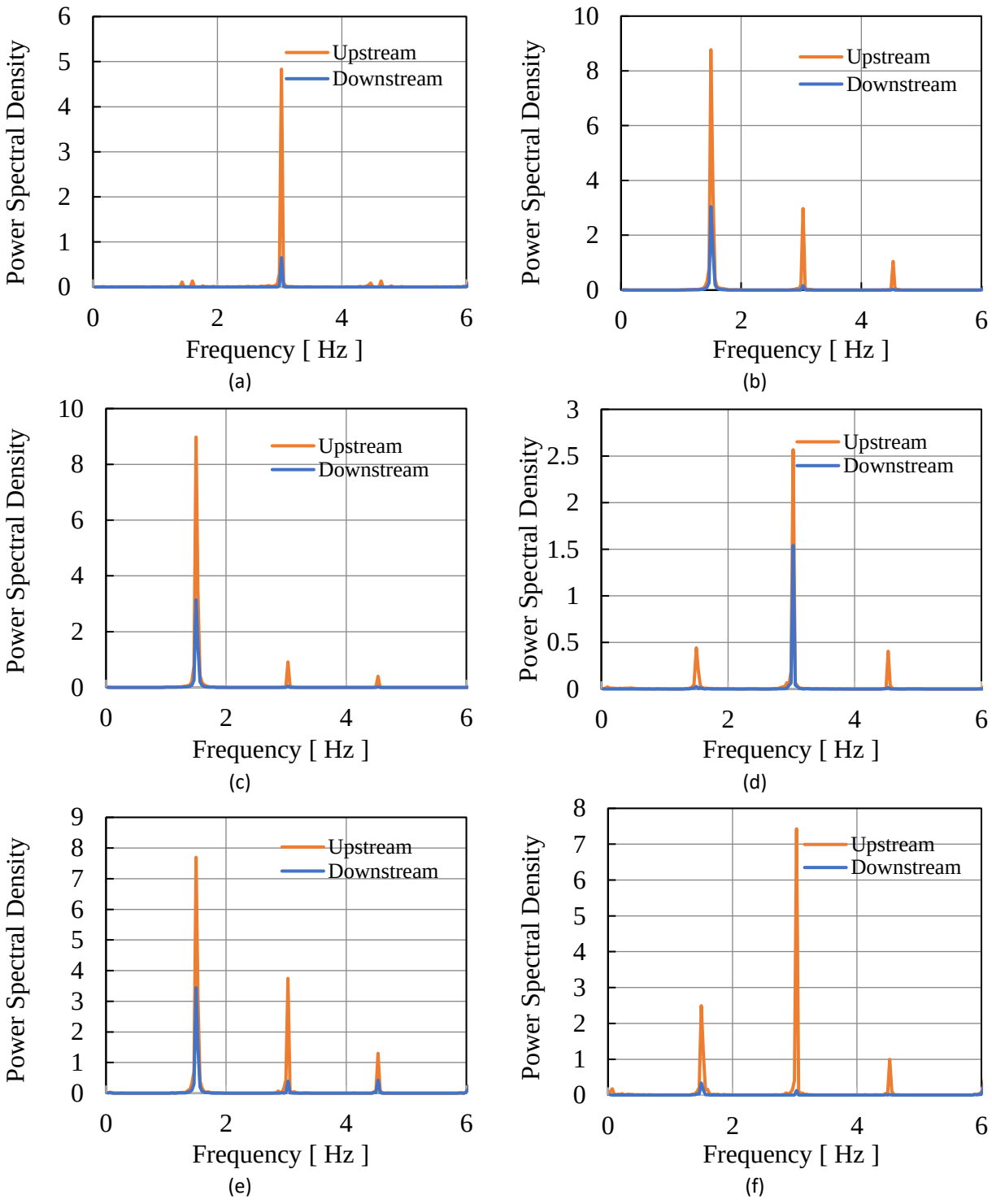
Power Spectral Density
Frequency [Hz]
Upstream
Downstream
(a)
(b)
(c)
(d)
(e)
(f)

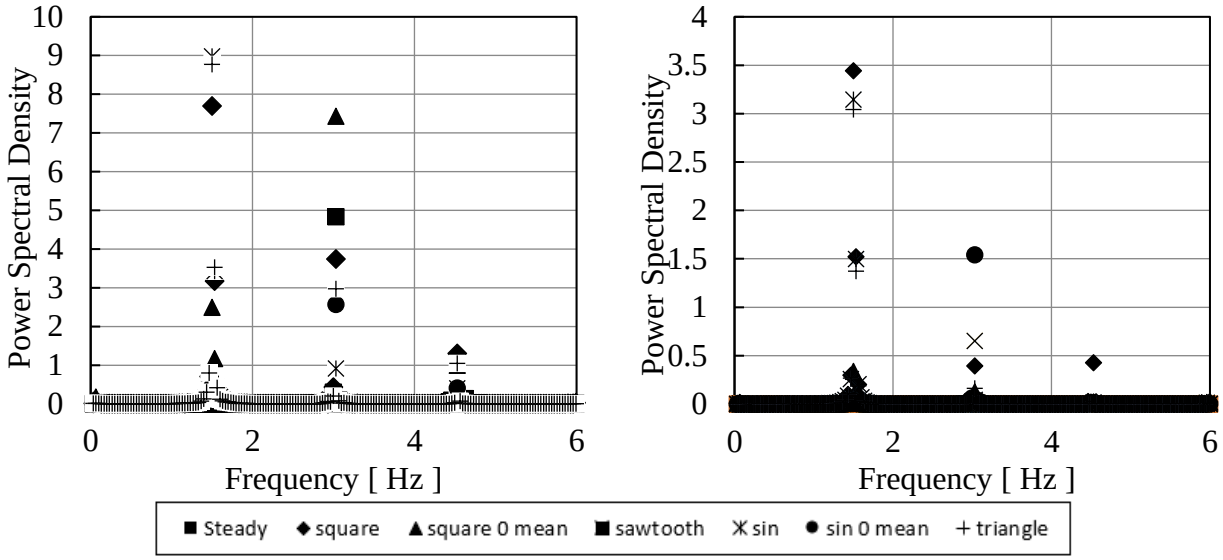

Fig. 22. Velocity in the domain inlet and downstream of the cylinder in the frequency domain for the (a) sawtooth, (b) triangular, (c) sine, (d) sine zero-mean, (e) square, and (f) square zero-mean waves and all results combined at the g) upstream and h) downstream positions

4.4 Optimization Results

Different waves were investigated to determine their effects on wall cooling. Optimization was conducted for each wave type to find the optimum wave frequency and amplitude. The investigated waves were sawtooth, triangular, sine, and square waves, with a mean velocity of 1 m/s and variable amplitude and frequency. The amplitude varied from 0.2 to 0.8 m/s, whereas the frequency varied from 2 to 12 Hz. Sine and square waves with zero mean were also considered.

The most efficient wave was the sawtooth wave, followed by the triangular wave, where the reductions in the wall temperature (cooling benefit) were 3.15% and 2.40% lower than that of the steady case, respectively. The worst wave was the sine wave with zero mean velocity, where the wall temperature was 1.68% higher than that in the steady case. The temperatures of the different optimum cases are listed in Table 8 and Figure 23.

Table 8
Optimum wave frequencies and amplitudes for different waveforms

Wave type	Amplitude	Frequency	Temp (K)	Temp difference (K)	Cooling benefit
Steady	0	0	378.951	0.00	0.00%
Sawtooth	0.9	11.72376	367.005	−11.95	3.15%
Triangle	0.9	12	369.853	−9.10	2.40%
Sine	0.9	12	370.698	−8.25	2.18%
Square	0.466242	9.574485	372.193	−6.76	1.78%
Square zero mean	0.466242	9.574485	372.193	−6.76	1.78%
Sine zero mean	0.9	2	385.299	6.35	−1.68%

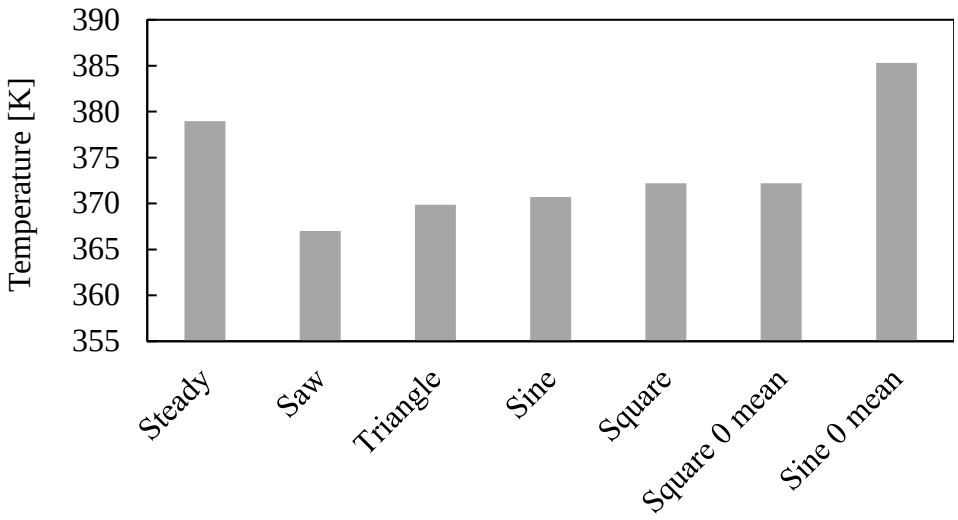

Fig. 23. Optimum temperatures for different waves measured after 3 min

The mass flow inlet to the domain was one of the main parameters that affected the cooling process. The basic hypothesis is that cooling is directly proportional to the mass flow. Hence, one must quantify the total air mass entering the domain and correlate it with the wall temperature reduction to examine this hypothesis. Thus, the mass flow rate was integrated for different waves for ¼, ½, and full cycles, and the results are listed in Table 9. The integration was done using the trapezoidal rule, and the time step used was 0.1 s. It was found that for the ¼ cycle, the triangular wave had the maximum total mass flow, followed by the sawtooth wave. However, for one complete cycle, the sawtooth wave surpassed the triangular wave because of the initial phase shift. Meanwhile, the sine zero-mean wave had the minimum total mass flow.

Table 9
Mass flow integration for different wave types

Wave type	After 1/4 cycle	After 1/2 cycle	After 1 cycle
Steady	1.6	3.3	6.3
Sine	2.114171	4.292912	6.300071
Sine zero mean	0.514171	0.992912	7.06E−05
Square	2.375	4.775	6.325
Square 0 mean	0.775	1.475	0.0025
Triangular	2.23854	4.526394	6.29958
Sawtooth	2.16146	3.273606	6.326483

Returning to the hypothesis mentioned earlier, Figure 24 shows that as the total mass flow integral for the ¼ cycle increased, the wall temperature decreased. These results were under the optimum conditions for each wave type individually. Note that the temperature axis (right) is flipped for ease of interpretation.

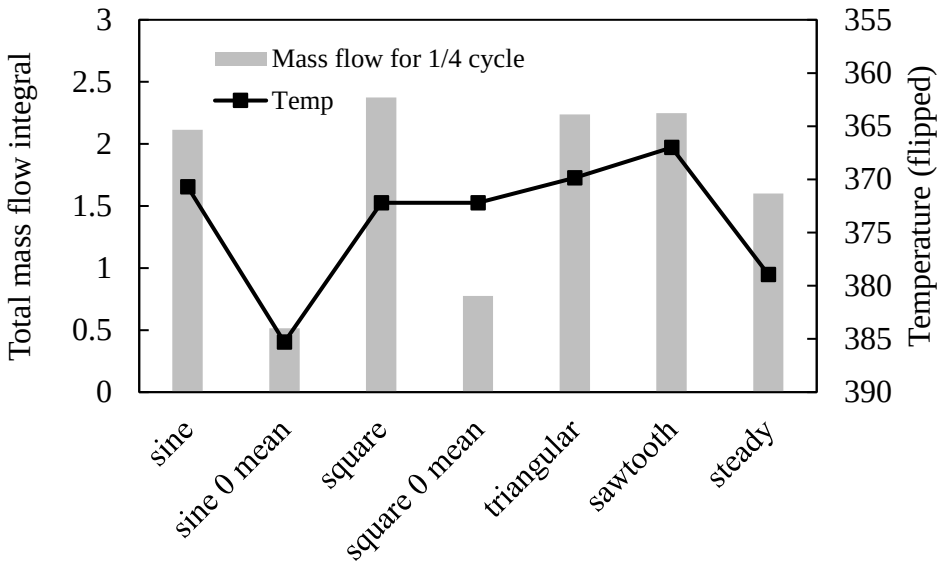

Fig. 24. Total mass inlet and wall temperature for different wave types under optimum conditions

Hence, the correlation between the total mass inlet and wall cooling was obtained using the Pearson correlation coefficient. The correlation coefficient is a statistical measure of the strength of the relationship between the relative movements of two variables, say *X* and *Y* [51].

$$r = \frac{\sum_i^n (x_i - \bar{x})(y_i - \bar{y})}{\sqrt{\sum_i^n (x_i - \bar{x})^2 \sum_i^n (y_i - \bar{y})^2}} \tag{7}$$

where *r* is the correlation coefficient, the variables with the subscript *i* are the values of such set, and the letters with overhead bars are the means of the values of such set. The values ranged between −1.0 and 1.0, where ±1.0 shows a perfect positive/negative correlation, whereas 0.0 shows no linear relationship between the two variables. The correlation coefficient, based on the mass flow of the ¼ cycle, was found to be −0.73. Hence, a good correlation was found between the total mass flow and the wall mean temperature. Thus, the hypothesis is acceptable. Also, this value became −0.55 when a complete cycle was used because of the inclusion of the negative part of the wave; hence, the integration only represents the mean mass flow.

5. Regression Modeling

In the general multiple regression model, there are pp independent variables:

$$y_i = B_0 + B_j x_{ij} + \epsilon_i \; for \; i = 1,2, \dots, p \tag{8}$$

where $y_i y_i$ represents the observations, xx are the independent variables, BB is the regression intercept. and $\epsilon\epsilon$ is the error. For ease of processing, this equation can be written in matrix form as

$$Y = \boldsymbol{X}B + \epsilon \tag{9}$$

The least squares parameter estimates were obtained from pp normal equations. The residual can be written as

$$\epsilon_i = y_i - \widehat{B}_\iota x_{ij} \tag{10}$$

In matrix notation, the normal equations are written as

$$(X^T X)\hat{B} = X^T Y \tag{11}$$

Hence, the regression intercept vector can be calculated from

$$\hat{B} = (X^T X)^{-1} X^T Y \tag{12}$$

The coefficient of determination (R^2) must be calculated to quantify the accuracy of the regression model. R^2 is a statistical measure in a regression model that determines the proportion of variance in the dependent variable that can be explained by the independent variable. In other words, R^2 shows how well the data fit the regression model. It is calculated from

$$R^2 = 1 - \frac{\sum_i^n (y_i - \widehat{y}_\iota)^2}{\sum_i^n (y_i - \bar{y})^2} \tag{13}$$

where y_i is the actual observation value, $\widehat{y}_\iota$ is the fitted value, and $\bar{y}$ is the mean value of the observations.

As one adds more variables to the model, the R^2 value of the new bigger model will always be greater than that of the smaller subset. This occurs because all the variables in the original model present their contribution to explain the dependent variable. Therefore, whatever new variable is added, it can only add to the variation that was already explained. Hence, the adjusted R^2 value comes to help. Adj-R^2 penalizes the total value for the number of terms in the model. Therefore, when comparing nested models, it is a good practice to look at the adj-R^2 value over R^2.

$$R^2_{\text{adj}} = 1 - \left(\frac{(1-R^2)(n-1)}{n-q}\right) \tag{14}$$

where n is the number of observations and q is the number of coefficients in the model.

Given the average wall temperatures for the different wave amplitudes, frequencies, and wave types, a regression model was used to estimate their contribution to wall cooling. The model equation used is the following:

$$\text{Temp} = A + B * \text{Amplitude} + C * \text{Frequency} + D * \text{Amplitude} * \text{Frequency} \tag{15}$$

The results of the coefficients for the different wave types are listed in Table 10. It is shown that all waves can be fitted well in the model equation except for the square wave, where their R^2 values are much less than 1. The most accurate fitting is that for the sine wave with zero mean, followed by that of the sawtooth wave. The wave frequency was found to slightly affect the cooling process, whereas the wave amplitude had a greater influence. Cooling was directly proportional to the amplitude in the sawtooth wave and sine wave with zero mean and slightly inversely proportional to the other waves. Meanwhile, the frequency was directly proportional to cooling for all types of waves except for both sine waves. Also, cooling was directly proportional to the multiplication of the wave amplitude and frequency, except for the sine wave with zero mean.

Table 10
Values of the coefficients of the regression model for different waveforms

Wave type	Coefficient A	Coefficient B	Coefficient C	Coefficient D	R^2
Sawtooth	380.96	−13.419	−0.0665	−0.12	0.9867
Triangular	378.729	0.508	−0.1604	−0.7011	0.9757
Sine	377.843	2.739	0.0124	−0.928	0.92
Sine zero mean	399.708	−17.152	0.0187	0.276	0.9877
Square	377.9299	1.9112	−0.1886	−0.542	0.4374
Square zero mean	377.092	3.898	−0.0828	−0.881	0.3743

6. Conclusions

Pulsating flow over a heated cylinder was investigated for seven different inlet velocity waveforms: steady, triangular, sawtooth, steady, sine, and square waves. The last two waves were investigated for two different mean velocities. The wave frequency varied from 2 to 12 Hz, and the amplitude varied from 0.2 to 0.8 m/s.

For constant wave frequency and amplitude, the most efficient wave in cooling was the sawtooth wave, where the average wall temperature after 30 s was 1.6K cooler than that of the forced convection case, followed by the triangular wave at 1.2K less. Moreover, for zero-mean mass flow rate waves, the square wave had better cooling performance than that of the sine wave.

After optimizing the frequency and amplitude for the different waves, the most efficient wave was found to be the sawtooth once again, with a temperature reduction of 12°C compared with that of the forced convection case, followed by the triangular case at 9°C less. This was because the sawtooth wave had a higher total mass flow per wave. Considering the zero-mean mass flow rate waves, the square wave again showed a better cooling performance than that of the sine wave.

By analyzing the waves at different frequencies and amplitudes, it was found that the wave amplitude had a greater role in cooling than that of the frequency. Also, the cooling was influenced by the first-order interaction between wave amplitude and frequency. The wave frequency was directly proportional to cooling for all types of waves except for the sine waves, whereas the relation between the wave amplitude and cooling depended on the wave type.

References

[1] Hantschk, C-C., and D. Vortmeyer. "Numerical simulation of self-excited thermoacoustic instabilities in a Rijke tube." *Journal of Sound and Vibration* 227, no. 3 (1999): 511-522. https://doi.org/10.1006/jsvi.1999.2296

[2] Föller, S., F. Selimefendigil, and W. Polifke. "Linear identification of the unsteady heat transfer of a cylinder in pulsating crossflow." In *International Conference on Jets, Wakes and Separated Flows*. 2008.

[3] Yu, Jiu-Yang, Wei Lin, and Xiao-Tao Zheng. "Effect on the flow and heat transfer characteristics for sinusoidal pulsating laminar flow in a heated square cylinder." *Heat and Mass Transfer* 50 (2014): 849-864. https://doi.org/10.1007/s00231-014-1294-4

[4] Molochnikov, V. M., N. I. Mikheev, A. N. Mikheev, and A. A. Paereliy. "Heat transfer from a cylinder in pulsating cross-flow." *Thermophysics and Aeromechanics* 24, no. 4 (2017): 569-575. https://doi.org/10.1134/S0869864317040084

[5] Saxena, Ashish, and Eddie Yin Kwee Ng. "Steady and pulsating flow past a heated rectangular cylinder (s) in a channel." *Journal of Thermophysics and Heat Transfer* 32, no. 2 (2018): 401-413. https://doi.org/10.2514/1.T5265

[6] Bhalla, Neelesh, and Amit Kumar Dhiman. "Pulsating flow and heat transfer analysis around a heated semi-circular cylinder at low and moderate Reynolds numbers." *Journal of the Brazilian Society of Mechanical Sciences and Engineering* 39 (2017): 3019-3037. https://doi.org/10.1007/s40430-017-0749-1

[7] Li, Guoneng, Youqu Zheng, Guilin Hu, Zhiguo Zhang, and Yousheng Xu. "Experimental study of the heat transfer enhancement from a circular cylinder in laminar pulsating cross-flows." *Heat Transfer Engineering* 37, no. 6 (2016): 535-544. https://doi.org/10.1080/01457632.2015.1060758

[8] Ji, Tae Ho, Seo Young Kim, and Jae Min Hyun. "Experiments on heat transfer enhancement from a heated square cylinder in a pulsating channel flow." *International Journal of Heat and Mass Transfer* 51, no. 5-6 (2008): 1130-1138. https://doi.org/10.1016/j.ijheatmasstransfer.2007.04.015

[9] Kikuchi, Yoshihiro, Hiroshi Suzuki, Masonori Kitagawa, and Ken-Ichiro Ikeya. "Effects of Pulsating Strouhal Number on Heat Transfer around a Heated Cylinder in Pulsating Cross-Flow." *JSME International Journal Series B Fluids and Thermal Engineering* 43, no. 2 (2000): 250-257. https://doi.org/10.1299/jsmeb.43.250

[10] Perwaiz, Jamshed, and T. E. Base. "Heat transfer from a cylinder and finned tube in a pulsating crossflow." *Experimental Thermal and Fluid Science* 5, no. 4 (1992): 506-512. https://doi.org/10.1016/0894-1777(92)90037-6

[11] Alimohammadi, S., P. Dinneen, T. Persoons, and D. B. Murray. "Thermal management using pulsating jet cooling technology." In *Journal of Physics: Conference Series*, vol. 525, no. 1, p. 012011. IOP Publishing, 2014. https://doi.org/10.1088/1742-6596/525/1/012011

[12] Fukue, Takashi, Koichi Hirose, and Natsuki Yatsu. "Basic study on flow and heat Transfer performance of pulsating air flow for application to electronics cooling." *Transactions of The Japan Institute of Electronics Packaging* 7, no. 1 (2014): 123-131. https://doi.org/10.5104/jiepeng.7.123

[13] Zhang, Hongna, Sining Li, Jianping Cheng, Zhiying Zheng, Xiaobin Li, and Fengchen Li. "Numerical study on the pulsating effect on heat transfer performance of pseudo-plastic fluid flow in a manifold microchannel heat sink." *Applied Thermal Engineering* 129 (2018): 1092-1105. https://doi.org/10.1016/j.applthermaleng.2017.10.124

[14] Zhan, Zengkun, Lixia Chen, Hongna Zhang, Chuandong Lin, Sining Li, Xiaobin Li, and Fengchen Li. "Numerical study on heat transfer enhancement by viscoelastic fluid pulsating laminar flow in rectangular microchannel heat sinks." *Applied Thermal Engineering* 213 (2022): 118734. https://doi.org/10.1016/j.applthermaleng.2022.118734

[15] Olayiwola, Bolaji O., and Peter Walzel. "Flow pulsation and modified duct surface for process heat transfer intensification." *International Journal of Chemical Reactor Engineering* 5, no. 1 (2007). https://doi.org/10.2202/1542-6580.1427

[16] Xu, Peng, Shuxia Qiu, MingZhou Yu, Xianwu Qiao, and Arun S. Mujumdar. "A study on the heat and mass transfer properties of multiple pulsating impinging jets." *International Communications in Heat and Mass Transfer* 39, no. 3 (2012): 378-382. https://doi.org/10.1016/j.icheatmasstransfer.2012.01.001

[17] Jung, Chuljae, and Sung Jin Kim. "Effects of oscillation amplitudes on heat transfer mechanisms of pulsating heat pipes." *International Journal of Heat and Mass Transfer* 165 (2021): 120642. https://doi.org/10.1016/j.ijheatmasstransfer.2020.120642

[18] Das, Sampad Gobinda, Suvanjan Bhattacharyya, Himadri Chattopadhyay, and Ali Cemal Benim. "Transport phenomenon of simultaneously developing flow and heat transfer in twisted sinusoidal wavy microchannel under pulsating inlet flow condition." *Heat Transfer Engineering* 43, no. 3-5 (2021): 410-422. https://doi.org/10.1080/01457632.2021.1875166

[19] Mishra, G., and R. P. Chhabra. "Influence of flow pulsations and yield stress on heat transfer from a sphere." *Applied Mathematical Modelling* 90 (2021): 1069-1098. https://doi.org/10.1016/j.apm.2020.10.003

[20] Luo, Xiangyu, Weichen Zhang, Haitao Dong, Amrit Kumar Thakur, Bing Yang, and Wensheng Zhao. "Numerical analysis of heat transfer enhancement of fluid past an oscillating circular cylinder in laminar flow regime." *Progress in Nuclear Energy* 139 (2021): 103853. https://doi.org/10.1016/j.pnucene.2021.103853

[21] Ding, Lin, Yuxiong Han, Zuomei Yang, Li Zhang, and Haoyu He. "Influence of upstream cylinder on flow-induced vibration and heat transfer of downstream cylinder." *International Journal of Thermal Sciences* 176 (2022): 107519. https://doi.org/10.1016/j.ijthermalsci.2022.107519

[22] Yawar, Arsalan, M. Ebrahem, S. Manzoor, N. A. Sheikh, and Muzaffar Ali. "Transient cross flow and heat transfer over a rotationally oscillating cylinder subjected to gust impulse." *International Journal of Heat and Mass Transfer* 137 (2019): 108-123. https://doi.org/10.1016/j.ijheatmasstransfer.2019.03.113

[23] Ghazanfarian, J., and M. R. H. Nobari. "A numerical study of convective heat transfer from a rotating cylinder with cross-flow oscillation." *International Journal of Heat and Mass Transfer* 52, no. 23-24 (2009): 5402-5411. https://doi.org/10.1016/j.ijheatmasstransfer.2009.06.036

[24] Fu, Wu-Shung, and Bao-Hong Tong. "Numerical investigation of heat transfer from a heated oscillating cylinder in a cross flow." *International Journal of Heat and Mass Transfer* 45, no. 14 (2002): 3033-3043. https://doi.org/10.1016/S0017-9310(02)00016-9

[25] Farahani, S. D., A. H. Rabiee, A. M. Zakinia, and Amir Mosavi. "A comparison of the pulsating and steady jets on flow-induced vibrations and thermal behavior of a sprung cylinder inside an isothermal channel." *Case Studies in Thermal Engineering* 30 (2022): 101761. https://doi.org/10.1016/j.csite.2022.101761

[26] Esfe, Mohammad Hemmat, Mehdi Bahiraei, Amirhesam Torabi, and Majid Valadkhani. "A critical review on pulsating flow in conventional fluids and nanofluids: Thermo-hydraulic characteristics." *International Communications in Heat and Mass Transfer* 120 (2021): 104859. https://doi.org/10.1016/j.icheatmasstransfer.2020.104859

[27] Ye, Qianhao, Yonghai Zhang, and Jinjia Wei. "A comprehensive review of pulsating flow on heat transfer enhancement." *Applied Thermal Engineering* 196 (2021): 117275. https://doi.org/10.1016/j.applthermaleng.2021.117275
[28] Mladin, E. C., and D. A. Zumbrunnen. "Local convective heat transfer to submerged pulsating jets." *International Journal of Heat and Mass Transfer* 40, no. 14 (1997): 3305-3321. https://doi.org/10.1016/S0017-9310(96)00380-8
[29] Poh, Hee Joo, Kurichi Kumar, and Arun S. Mujumdar. "Heat transfer from a pulsed laminar impinging jet." *International Communications in Heat and Mass Transfer* 32, no. 10 (2005): 1317-1324. https://doi.org/10.1016/j.icheatmasstransfer.2005.07.012
[30] Coulthard, Sarah M., Ralph J. Volino, and Karen A. Flack. "Effect of jet pulsing on film cooling-part I: effectiveness and flow-field temperature results." *Journal of Turbomachinery* 129, no. 2 (2007): 232-246. https://doi.org/10.1115/1.2437231
[31] Xu, Chong, Shanglong Xu, Zuyuan Wang, and Daiwei Feng. "Experimental investigation of flow and heat transfer characteristics of pulsating flows driven by wave signals in a microchannel heat sink." *International Communications in Heat and Mass Transfer* 125 (2021): 105343. https://doi.org/10.1016/j.icheatmasstransfer.2021.105343
[32] Li, Ping, Dingzhang Guo, and Ruirui Liu. "Mechanism analysis of heat transfer and flow structure of periodic pulsating nanofluids slot-jet impingement with different waveforms." *Applied Thermal Engineering* 152 (2019): 937-945. https://doi.org/10.1016/j.applthermaleng.2019.01.086
[33] Zargarabadi, Mehran Rajabi, Ehsan Rezaei, and Babak Yousefi-Lafouraki. "Numerical analysis of turbulent flow and heat transfer of sinusoidal pulsed jet impinging on an asymmetrical concave surface." *Applied Thermal Engineering* 128 (2018): 578-585. https://doi.org/10.1016/j.applthermaleng.2017.09.059
[34] Zhang, Yanyao, Ping Li, and Yonghui Xie. "Numerical investigation of heat transfer characteristics of impinging synthetic jets with different waveforms." *International Journal of Heat and Mass Transfer* 125 (2018): 1017-1027. https://doi.org/10.1016/j.ijheatmasstransfer.2018.04.120
[35] Geng, Liping, Chuanbo Zheng, and Jingwei Zhou. "Heat transfer characteristics of impinging jets: The influence of unsteadiness with different waveforms." *International Communications in Heat and Mass Transfer* 66 (2015): 105-113. https://doi.org/10.1016/j.icheatmasstransfer.2015.05.017
[36] Mohammadpour, Javad, Mehran Rajabi-Zargarabadi, Arun S. Mujumdar, and Hadi Ahmadi. "Effect of intermittent and sinusoidal pulsed flows on impingement heat transfer from a concave surface." *International Journal of Thermal Sciences* 76 (2014): 118-127. https://doi.org/10.1016/j.ijthermalsci.2013.08.018
[37] Mladin, E. C., and D. A. Zumbrunnen. "Local convective heat transfer to submerged pulsating jets." *International Journal of Heat and Mass Transfer* 40, no. 14 (1997): 3305-3321. https://doi.org/10.1016/S0017-9310(96)00380-8
[38] Mladin, E. C., and D. A. Zumbrunnen. "Dependence of heat transfer to a pulsating stagnation flow on pulse characteristics." *Journal of Thermophysics and Heat Transfer* 9, no. 1 (1995): 181-192. https://doi.org/10.2514/3.645
[39] Sheriff, H. S., and D. A. Zumbrunnen. "Effect of flow pulsations on the cooling effectiveness of an impinging jet." *Journal of Heat and Mass Transfer* 116, no. 4 (1994): 886-895. https://doi.org/10.1115/1.2911463
[40] Demircan, Tolga, and Hasmet Turkoglu. "The numerical analysis of oscillating rectangular impinging jets." *Numerical Heat Transfer, Part A: Applications* 58, no. 2 (2010): 146-161. https://doi.org/10.1080/10407782.2010.496669
[41] Bazdidi-Tehrani, Farzad, Mahdi Karami, and Mehdi Jahromi. "Unsteady flow and heat transfer analysis of an impinging synthetic jet." *Heat and Mass Transfer* 47 (2011): 1363-1373. https://doi.org/10.1007/s00231-011-0801-0
[42] Jena, Siddharth, and Ajay Gairola. "Novel Boundary Conditions for Investigation of Environmental Wind Profile Induced due to Raised Terrains and Their Influence on Pedestrian Winds." *Journal of Advanced Research in Applied Sciences and Engineering Technology* 27, no. 1 (2022): 77-85. https://doi.org/10.37934/araset.27.1.7785
[43] Ariffin, Ahmad Hamdan, and Kamarul Ariffin Ahmad. "Computational Fluid Dynamic (CFD) Simulation of Synthetic Jet Cooling: A Review." *Journal of Advanced Research in Fluid Mechanics and Thermal Sciences* 72, no. 2 (2020): 103-112. https://doi.org/10.37934/arfmts.72.2.103112
[44] Gaheen, Osama A., Mohamed A. Aziz, M. Hamza, Hoda Kashkoush, and Mohamed A. Khalifa. "Fluid and Structure Analysis of Wind Turbine Blade with Winglet." *Journal of Advanced Research in Fluid Mechanics and Thermal Sciences* 90, no. 1 (2022): 80-101. https://doi.org/10.37934/arfmts.90.1.80101
[45] Alfarawi, Suliman, Azeldin El-sawi, and Hossin Omar. "Exploring Discontinuous Meshing for CFD Modelling of Counter Flow Heat Exchanger." *Journal of Advanced Research in Numerical Heat Transfer* 5, no. 1 (2021): 26-34.
[46] Yaseen, Duna T., Amani J. Majeed, and Muneer A. Ismael. "Cooling of hot cylinder placed in a flexible backward-facing step channel." *Thermal Science and Engineering Progress* 33 (2022): 101364. https://doi.org/10.1016/j.tsep.2022.101364

[47] Aziz, Mohamed A., and Osama A. Gaheen. "Effect of the isothermal fins on the natural convection heat transfer and flow profile inside a vertical channel with isothermal parallel walls." *SN Applied Sciences* 1, no. 10 (2019): 1310. https://doi.org/10.1007/s42452-019-1232-7

[48] Gaheen, Osama A., Ernesto Benini, Mohamed A. Khalifa, M. E. El-Salamony, and Mohamed A. Aziz. "Experimental investigation on the convection heat transfer enhancement for heated cylinder using pulsated flow." *Thermal Science and Engineering Progress* 26 (2021): 101055. https://doi.org/10.1016/j.tsep.2021.101055

[49] Gaheen, Osama A., Ernesto Benini, Mohamed A. Khalifa, and Mohamed A. Aziz. "Pneumatic cylinder speed and force control using controlled pulsating flow." *Engineering Science and Technology, an International Journal* 35 (2022): 101213. https://doi.org/10.1016/j.jestch.2022.101213

[50] El-Salamony, Mostafa, Mohamed Aziz, Ernesto Benini, and Osama Gaheen. "Optimization Study of Unsteady Flow Affecting on Cooling a Heated Cylinder." In *2021 3rd Novel Intelligent and Leading Emerging Sciences Conference (NILES)*, pp. 175-178. IEEE, 2021. https://doi.org/10.1109/NILES53778.2021.9600557

[51] Oehlert, Gary W. *A first course in design and analysis of experiments*. University of Minnesota, 2010.